TECHNICAL NOTES

무인항공기를 이용한 절리사면의 안정성평가 계측장비 개발

이현철*, 권기문, 문창은, 조영훈

주식회사 구주엔지니어링

Measurement Equipment Development of Stability Evaluation for Joint Slope using Unmaned Aerial Vehicle

Hyun Chol Lee*, Ki Mun Kwon, Chang Eun Moon, and Yeong Hun Jo
Guju Engineering Inc.

*Corresponding author: lhc0414@chol.com

ABSTRACT

In order to interpret rock slope safely and effectively, the mechanical properties of the rock must be carefully investigated. However, due to the limitations of clinometer usage, a new measure of measurement is required to complement these limitations. In this study, a measuring device was developed to analyze the characteristics of joint orientation, and to apply the orientation of joint to the field. The developed measuring equipment is divided into analysis software and hardware. The hardware was composed of a measuring module that measures the joint orientation of rock and a transport module that transmits the measurement data. The software was developed to analyze the orientation of the joint from the data obtained from the measuring module and is named Drone Joint Orientation Survey Measurement. The developed measuring equipment was well field capable if it could not be measured by the inspector, such as in areas where access was difficult, and was capable of effectively analyzing the lab test results for the orientation of the joint.

Keywords: Unmaned Aerial Vehicle, Joint measurement system, Joint orientation, Xbee

초록

암반사면을 안전하고 효과적으로 해석하기 위해서 암반의 역학적 특성을 면밀하게 조사해야 한다. 하지만 클리노미터를 사용한 절리조사의 한계점으로 인해 이를 보완한 새로운 측정법의 연구가 필요하다. 본 연구에서는 절리방향의 특성을 분석하기 위해 절리의 방향성을 현장에 적용할 수 있는 절리조사 측정장비를 개발하였다. 개발된 측정장비는 해석 소프트웨어와 하드웨어로 구분된다. 하드웨어는 암반 절리 방향성을 측정하는 측정모듈, 측정자료를 전송하는 전송모듈로 구성되었다. 소프트웨어는 측정모듈을 통해 얻은 데이터로부터 절리의 방향성을 분석하기 위해 개발하였으며 Drone Joint Orientation Survey Measurement로 명명하였다. 개발된 측정장비는 접근이 어려운 지역 등 조사자가 측정할 수 없는 경우에 현장적용성이 양호하며 절리의 방향성에 대한 실내시험결과를 효과적으로 분석할 수 있었다.

핵심어: 무인항공기, 절리측정시스템, 절리방향성, 지그비

1. Introduction

In general, rock analysis exposed to the surface is classified as a stable analysis considering the joint orientation and the mechanical characteristics. This is because the stability of the rock is associated with the orientation of the joint and its mechanical properties.

The characteristics of the rock joint structure are derived from the analysis of the joint surface and the statistical analysis after making contact with the joint surface, such as the survey of the scanline, the investigation of the window, and the investigation by the clinometer (Son et al., 2014).

Currently, the use of long-distance survey techniques using photogrammetry techniques and laser scanner methods is increasing, but this is due to the lack of efficiency in analysis of joint structures in large rock and the subjective opinions of the inspector (Moffitt and Mikhail, 1980).

To solve these problems, this study attempted to develop a device for measuring the field joint orientation for the analysis of joint slope. The shrink-level measurement device is divided into hardware and analytic software. The hardware was configured with drones, arduino uno, servo motor, joint orientation measuring module, and wireless transmission module of measurement data to measure the direction of joint structures. The software has been developed to analyze the orientation of joint by printing the data obtained from the measuring module on-screen, and it is called Drone Joint Survey.

The purpose of this study is to develop a device to measure the joint orientation, a mechanical feature of the rock, and to measure the joint orientation module, in order to safely and effectively interpret the rock slope through compare with the existing clinometer.

2. Theoretical Background

For the purpose of evaluating the mechanical stability, the measurements are made on the discontinuous surfaces, such as the joint, and the consequences are likely to be the potential failure aspects of the slope based on the properties of these discontinuous surfaces (Lee, 2016).

The dip angle and dip direction, especially on the discontinuous surface, are the major factors that determine the type of failure upon the collapse of the slope.

A compass clinometer is used to measure the joint surface. (compass clinometer, geological compass, clino-compass, inclinometer with compass etc.). Since the direction of the slope on the clinometer must be measured in a horizontal plane, it is necessary to adjust the equipment horizontally while the joint surface is closely attached to it. Measure the angle after the instructions for compass are stabilized.
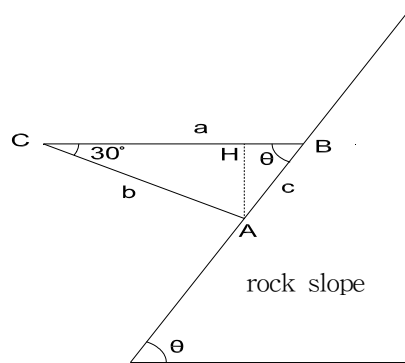
Fig. 1. Measurement diagram using drone
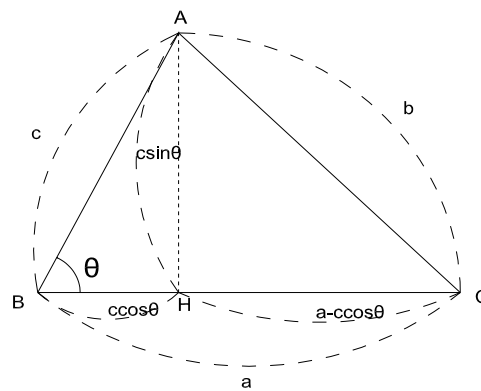
Fig. 2. Calculation diagram of degree

Fig. 1 shows a schematic diagram of the joint orientation measurement of rock slope using drones. At point C, hovering drones to measure the value of the horizontal distance a to the rock slope through the ultrasonic sensors and rotate the measured angle, 30° A, in a clockwise direction from the horizontal plane using the servo motor.

Determine the distance value of c that connects the two points on the slope (A, B) and the second point (A) by forming a triangle with each other and using the following expression.

Determine the value of the angle of inclination (θ) by using the triangle's second cosine law in Fig. 2.

$$b^2 = a^2 + c^2 - 2ac\cos\theta$$

$$\cos\theta = \frac{a^2 + c^2 - b^2}{2ac}$$

$$\theta = \cos^{-1}\left(\frac{a^2 + c^2 - b^2}{2ac}\right)$$

(1)

The slope direction of the slope of rock slope joint is calculated from the angle of euler. The rotation order is ZYX (Roll-Pitch-Yaw). Calculate the rotation results of the target coordinate system against the reference coordinate system as

follows.

First, rotate the reference coordinate system about the X-axis (Yaw rate) : $R_x(\phi)$

Second, rotate the reference coordinate system about the Y axis (pitch) : $R_y(\theta)$

Third, rotate the reference coordinate system about the Z axis (Roll). : $R_z(\psi)$

$$R_{xyz} = R_z(\psi)R_y(\theta)R_x(\varnothing)$$
$$= \begin{bmatrix} \cos\theta\cos\psi & \sin\varnothing\sin\theta\cos\psi - \cos\varnothing\sin\psi & \cos\varnothing\sin\theta\cos\psi + \sin\varnothing\sin\psi \\ \cos\theta\sin\psi & \sin\varnothing\sin\theta\sin\psi + \cos\varnothing\cos\psi & \cos\varnothing\sin\theta\sin\psi - \sin\varnothing\cos\psi \\ -\sin\theta & \sin\varnothing\cos\theta & \cos\varnothing\cos\theta \end{bmatrix} \tag{2}$$

$$R_x(\Phi) = \begin{bmatrix} 1 & 0 & 0 \\ 0 & \cos\varnothing & -\sin\varnothing \\ 0 & \sin\varnothing & \cos\varnothing \end{bmatrix} \tag{3}$$

$$R_y(\theta) = \begin{bmatrix} \cos\theta & 0 & \sin\theta \\ 0 & 1 & 0 \\ -\sin\theta & 0 & \cos\theta \end{bmatrix} \tag{4}$$

$$R_z(\Psi) = \begin{bmatrix} \cos\psi & -\sin\psi & 0 \\ \sin\psi & \cos\psi & 0 \\ 0 & 0 & 1 \end{bmatrix} \tag{5}$$

It is possible to calculate the euler angle from the rotation matrix R as follows. The elements in row i and column j of matrix R are used in the following expression.

$$R = \begin{bmatrix} r_{11} & r_{12} & r_{13} \\ r_{21} & r_{22} & r_{23} \\ r_{31} & r_{32} & r_{33} \end{bmatrix} \tag{6}$$

When θ is $(-\pi/2, \pi/2)$:

$\psi = atan2(r_{21}, r_{11})$

$\theta = asin(-r_{31})$ $\tag{7}$

$\phi = atan2(r_{32}, r_{33})$

When θ is $(\pi/2, 3\pi/2)$:

$$\psi = atan2\left(-r_{21}, -r_{11}\right)$$
$$\theta = asin\left(-r_{31}\right) \tag{8}$$
$$\phi = atan2\left(-r_{32}, -r_{33}\right)$$

When the pitch angle is near $\pi/2$, the $\cos\theta \approx 0$. Calculate it as follows.

$$
\begin{aligned}
r_{23} - r_{12} &= (\sin\theta + 1)\sin(\psi - \phi) \\
r_{13} + r_{22} &= (\sin\theta + 1)\cos(\psi - \phi) \\
r_{23} + r_{12} &= (\sin\theta - 1)\sin(\psi + \phi) \\
r_{13} - r_{22} &= (\sin\theta - 1)\cos(\psi + \phi)
\end{aligned} \tag{9}
$$

$$
\begin{aligned}
\psi &= atan2\left(r_{23} + r_{12}, r_{13} - r_{22}\right) \\
\theta &= asin\left(-r_{31}\right) \\
\phi &= \psi - atan2\left(r_{23} - r_{12}, r_{13} + r_{22}\right)
\end{aligned} \tag{10}
$$

3. Joint Survey System

3.1 Composition and Principle of system

In this study, data acquisition and analysis was performed using sketch developed by SmartProjects company. The system consists of Arduino Uno, Sensor modules, Xbee modules, and Blynk. Fig. 3 shows the schematic diagram of the joint survey system.

3.2 Arduino Uno

Arduino Uno uses Atmel's 16 MHz microcontroller ATmega 328 capable of connecting multiple peripheral devices across a total of 20 I/O pins, providing connectivity and Table 1 presents technical specifications for the Arduino Uno (Simon, 2011).

3.3 9 Axes Motion Sensor

It is based on Bosch's BNO055 absolute orientation sensor, it runs a 3-axes 14-bit accelerometer, 3-axes 16-bit gyroscope, 3-axes earth magnetism, and BSX 3.0 FusionLib Software. In this study, measurements from a 9-axis motion sensor are used to determine the dip direction of the rock slope. Table 2 shows the technical specifications for the 9 Axes Motion Shield.
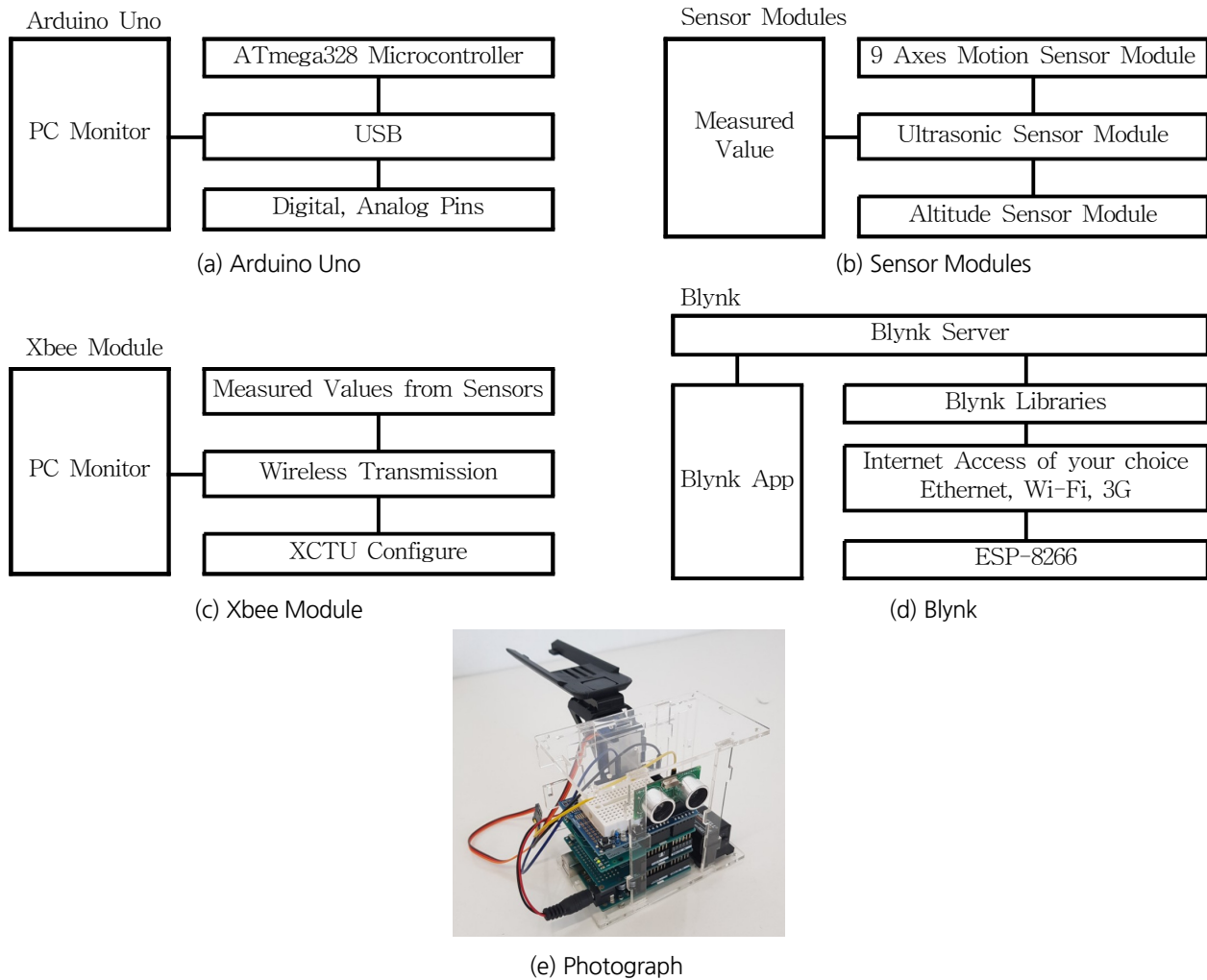
Arduino Uno

PC Monitor	ATmega328 Microcontroller
	USB
	Digital, Analog Pins

(a) Arduino Uno

Sensor Modules

Measured Value	9 Axes Motion Sensor Module
	Ultrasonic Sensor Module
	Altitude Sensor Module

(b) Sensor Modules

Xbee Module

PC Monitor	Measured Values from Sensors
	Wireless Transmission
	XCTU Configure

(c) Xbee Module

Blynk

Blynk Server	
Blynk App	Blynk Libraries
	Internet Access of your choice Ethernet, Wi-Fi, 3G
	ESP-8266

(d) Blynk

(e) Photograph

Fig. 3. Conceptual diagram of the joint survey System

Table 1. Technical Specification (Arduino Uno)

Division	Specifications
Microcontroller	ATmega328P
Operating Voltage	5 V
Digital I/O Pins	14(of which 6 provide PWM output)
DC Current per I/O Pin	20 mA
Flash Memory	32KB(ATmega328P) of which 0.5KB used by bootloader
Clock Speed	16 MHz

Table 2. Technical Specification (9 Axes Motion Shield)

Division	Specifications
Chip based	BOSCH Sensortech BNO055
Thinker Kit interface	2x TWI, 2x OUT, 2x IN
Motion Sensors	Triaxial accelerometer, Triaxial gyroscope, Triaxial geomagnetic
Fusion Engine	32-bit microcontroller with BSX3.0 FusionLib
Operating Voltage	5 / 3.3 V

3.4 Ultrasonic Sensor

The ultrasonic sensor module is HC-SR04, which measures 4 meters and has a measuring accuracy of 2 mm. An ultrasonic module consists of a transmission unit, a reception module, and a regulating circuit. In this study, ultrasonic sensors were used to measure the linear distance between the target rock slope and the measuring device. Table 3 shows the technical specifications for the ultrasonic sensor.

Table 3. Technical Specification (Ultrasonic Sensor)

Division	Specifications
Operating Voltage	DC 5V
Operating Current	15 mA
Operating Frequency	40 Hz
Measuring Angle	15 degree
Trigger Input Signal	10us TTL pulse

3.5 XBee Sensor

XBee, a communications network module based on the NFC method, is grouped into one-to-one communication, star topology and mesh type topology. The XBee module used in this study applied the Zigbee communication protocol, while the topology applied one-to-one communication. Table 4 shows the technical specifications for the xbee module.

Table 4. Technical Specification (XBee®/XBee-PRO® ZB RF Modules Datasheet,2010)

Division	Specifications
Transceiver Chipset	silicon Labs EM357 SoC
Data Rate	RF 250 Kpbs, Serial up to 1 Mbps
Outdoor / RF Line-of-sight Range	2 miles / 3200 m
Transmit Power	63 mW(+18dBm)
Receiver Sensitivity (1% per)	-101 dBm
Serial Data Interface	UART, SPI
Configuration Method	API or AT commands, local or over-the-air (OTA)
Antenna Options	PCB Antenna, U.FL Connector, RPSMA Connector
CPU / Clock Speed	HCS08 / up to 50.33 MHz
Protocol	ZigBee Pro 2007
Encryption	128-bit AES
Reliable Pack Delivery	Retries / Acknowledgements
IDS	PAN ID and addresses, cluster IDS and endpoints
Supply Voltage	2.7 to 3.6 V

3.6 Software of data acquired

Arduino's integrated development environment is a cross-platform application software developed based on Java and C, which is capable of compiling and uploading, and using C ++ language base for arduino operation (Hagan, 1980).

In this study, using sketches, data from both the Arduino Uno and the sensors were printed on the mobile computer.

3.7 Servo Motor

With TowerPro's SG-90 product, SG-90 is a small, lightweight product with a high output power. The servo can rotate about 180 degrees and is operated by three wires. It is used in this study to adjust the angle of the Drone Measure system. Table 5 lists technical specifications for SG-90.

Table 5. Technical Specification (SG-90)

Division	Specifications
Weight	9 g
Dimension	22.2 × 11.8 × 31 mm approx
Stall torque	1.8 kgf · cm
Operating speed	0.1s / 60 degree
Operating Voltage	4.8 V (~5V)
Dead band width	10 μs
Temperature range	0°C - 55°C

3.8 Unmaned Aerial Vehicle

It is a DJI's MAVIC PRO product, which uses forward and downstream vision sensors to accurately hovering rooms and satellites where they are not captured, and also maintains a fixed altitude on the uneven terrain. Table 6 shows the technical specifications for the MAVIC PRO.

Table 6. Technical Specification (MAVIC PRO)

Division	Specifications
Flight time	27 mins
Control range	7 km
Speed	65 km/h
Gimbal	3-axis
Video resolution	4K
Camera resolution	12 MP

3.9 ESP 8266

ESP 8266 is a micro-controller designed by Espressif Systems, and since a large number of ESP-xx modules operate only at 3.3 V, a 3.3 V power supply is required.

The GPIO (General Purpose Input Output) is a pin that can be controlled by the ESP 8266 module, like the pin in the Arduino, with a different number of pins available for each ESP-xx module. Table 7 lists technical specifications for ESP 8266.

Table 7. Technical Specification (ESP8266)

Division	Specifications
Voltage	3.3 V
Current consumption	10 uA − 170 mA
Flash memory attachable	16MB max (512K normal)
Processor	Tensilica L106 32 bit
Processor speed	80-160 MHz
RAM	32 K + 80 K
GPIOs	17 (multiplexed with other functions)
ADC (Analog to Digital)	1 input with 1024 step resolution
802.11 support	b/g/n/d/e/i/k/r
Maximum concurrent TCP connections	5

3.10 Blynk

Blynk is a platform that enables iOS and Android applications to control the makers of IoT devices such as Arduino and Raspberry Pies, and it is a platform that supports virtual, hardware-to-hardware connectivity.

4. Test Result

4.1 Result of Joint Data

For the purpose of making use of the joint survey system applied to this study, the dip angle was increased from 50° to 10° for each pair of surfaces, and measured from 10° to 90° for the dip direction. In the case of a 50° dip angle, the dip direction is measured from 90° to 140° and examined until the angle is 80°.

In the lab model test, the results of measurements using a clinometer were compared with the results obtained by a joint survey system. Fig. 4 shows the hardware configuration diagrams of the joint survey system. Fig. 5 represents a conventional survey device.

In this study, the data from lab tests were used to calculate the orientation of the joint and compared to the actual joint data

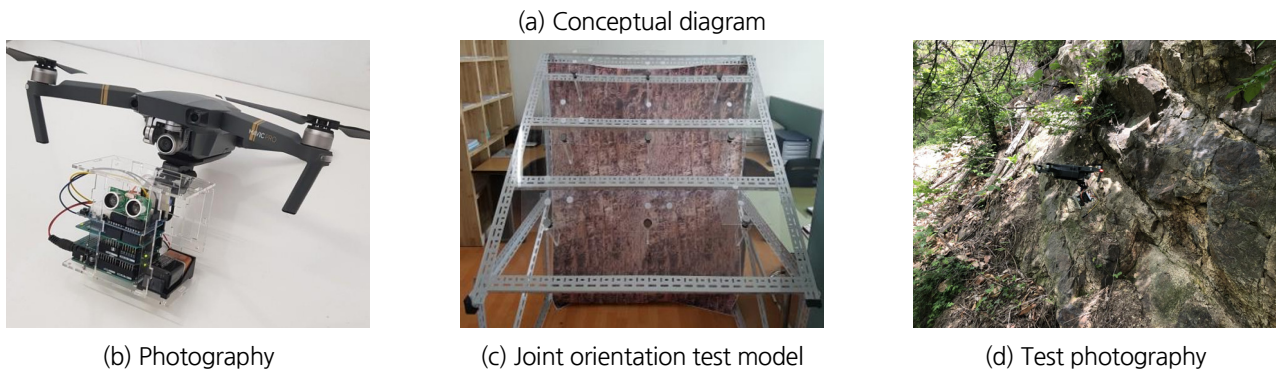obtained using the clinometer and mobile application.

① Arduino Uno
② Power Supply
③ Arduino 9 axes motion shield
④ Arduino wireless SD shield
⑤ Arduino proto shield
⑥ ESP-8266
⑦ Ultrasonic sensor
⑧ SG-90

(a) Conceptual diagram

(b) Photography

(c) Joint orientation test model

(d) Test photography
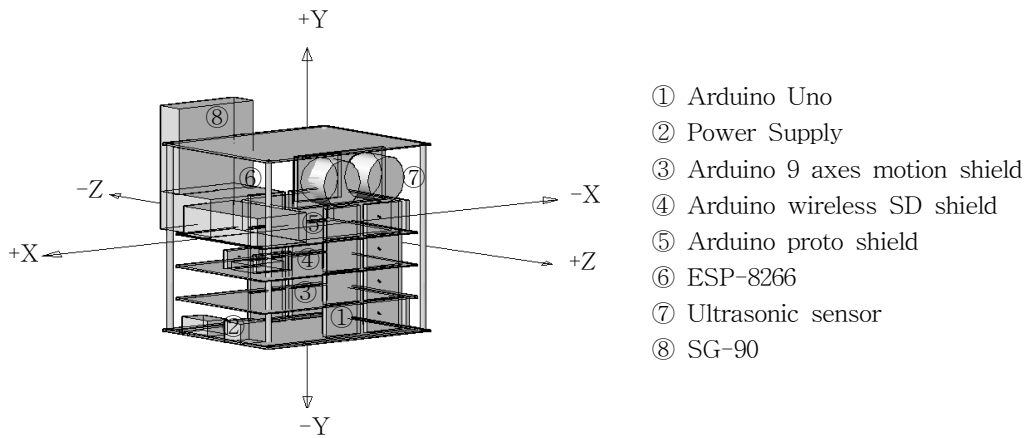
Fig. 4. Joint orientation test apparatus

(a) Clinometer

(b) Mobile application

Fig. 5. Clinometer and Mobile application

4.2 Reliability Analysis of Data

40 joints and 20 joints were selected to directly compare the joint orientation and to analyze reliability in the lab test and in the field test. As a result of the measurement error in the dip angle and the measured error in the dip direction of the slope of the clinometer are $\pm 5°$ and $\pm 10°$ respectively (Ewan and West, 1981), the machine error in the clinometer may be produced in $\pm 1°$ to $2°$. It has been analyzed that no data exceeds the tolerance range (dip : $\pm 7°$, dip direction : $\pm 12°$) set in this study (Park et al., 2015).

Table 8. Comparison of each joint orientation in the lab test (Clinometer and Drone Measure System and Mobile application)

(Unit : degree,°)

No.	Clinometer (a) Dip	Clinometer (a) Dip Direction	Drone Measure System (b) Dip	Drone Measure System (b) Dip Direction	Mobile application (c) Dip	Mobile application (c) Dip Direction	Difference (a:b) Dip	Difference (a:b) Dip Direction	Difference (b:c) Dip	Difference (b:c) Dip Direction
1	51	134.00	48.11	128.61	50	131.00	2.89	5.39	1.89	2.39
2	49	118.00	45.34	123.56	49	120.00	3.66	5.56	3.66	3.56
3	50	123.00	47.26	115.65	51	121.00	2.74	7.35	3.74	5.35
4	49	107.00	52.48	101.66	51	108.00	3.48	5.34	1.48	6.34
5	49	100.00	53.54	107.31	50	102.00	4.54	7.31	3.54	5.31
6	51	101.00	48.65	94.42	50	99.00	2.35	6.58	1.35	4.58
7	50	98.00	46.12	105.09	49	100.00	3.88	7.09	2.88	5.09
8	50	118.00	47.33	114.56	49	117.00	2.67	3.44	1.67	2.44
9	49	122.00	46.26	117.13	50	120.00	2.74	4.87	3.74	2.87
10	49	126.00	53.89	131.65	50	125.00	4.89	5.65	3.89	6.65
11	58	132.00	54.46	128.35	59	130.00	3.54	3.65	4.54	1.65
12	60	117.00	57.65	121.06	60	119.00	2.35	4.06	2.35	2.06
13	59	116.00	63.79	110.71	60	116.00	4.79	5.29	3.79	5.29
14	60	96.00	57.46	102.49	61	98.00	2.54	6.49	3.54	4.49
15	59	94.00	53.12	100.74	61	95.00	5.88	6.74	7.88	5.74
16	61	103.00	63.42	98.85	59	101.00	2.42	4.15	4.42	2.15
17	60	102.00	56.21	97.56	60	103.00	3.79	4.44	3.79	5.44
18	60	126.00	57.68	121.98	60	123.00	2.32	4.02	2.32	1.02
19	61	127.00	64.31	132.67	58	129.00	3.31	5.67	6.31	3.67
20	59	130.00	63.36	125.64	60	130.00	4.36	4.36	3.36	4.36
21	70	122.00	65.34	126.11	71	123.00	4.66	4.11	5.66	3.11
22	71	109.00	65.88	115.87	70	110.00	5.12	6.87	4.12	5.87
23	70	107.00	66.13	102.64	69	108.00	3.87	4.36	2.87	5.36
24	69	114.00	75.99	119.11	68	112.00	6.99	5.11	7.99	7.11
25	71	97.00	75.89	102.35	70	98.00	4.89	5.35	5.89	4.35
26	71	95.00	66.23	99.65	70	96.00	4.77	4.65	3.77	3.65
27	71	109.00	67.94	113.17	71	109.00	3.06	4.17	3.06	4.17
28	69	117.00	74.10	112.34	69	118.00	5.10	4.66	5.1	5.66
29	70	130.00	74.54	125.61	70	129.00	4.54	4.39	4.54	3.39
30	69	122.00	71.64	126.74	68	120.00	2.64	4.74	3.64	6.74
31	79	127.00	81.98	131.45	79	129.00	2.98	4.45	2.98	2.45
32	81	129.00	78.25	124.99	80	128.00	2.75	4.01	1.75	3.01
33	80	112.00	82.33	109.35	80	110.00	2.33	2.65	2.33	0.65
34	80	100.00	84.09	104.32	81	100.00	4.09	4.32	3.09	4.32
35	81	97.00	79.02	100.11	81	98.00	1.98	3.11	1.98	2.11
36	79	93.00	83.29	97.36	79	95.00	4.29	4.36	4.29	2.36
37	79	107.00	76.33	101.64	78	110.00	2.67	5.36	1.67	8.36
38	80	108.00	84.99	111.28	80	106.00	4.99	3.28	4.99	5.28
39	81	123.00	76.87	120.36	80	120.00	4.13	2.64	3.13	0.36
40	80	115.00	83.07	117.84	81	117.00	3.07	2.84	2.07	0.84
	Average Error						3.70	4.82	3.63	3.99

Table 9. Comparison of each joint orientation in the field test (Clinometer and Drone Measure System and Mobile application)

(Unit : degree,°)

No.	Clinometer (a)		Drone Measure System (b)		Mobile application (c)		Difference (a:b)		Difference (b:c)	
	Dip	Dip Direction	Dip	Dip Direction	Dip	Dip Direction	Dip	Dip Direction	Dip	Dip Direction
1	60	276.00	51.82	274.35	61	277.00	8.18	1.65	9.18	2.65
2	64	264.00	69.34	260.12	65	262.00	5.34	3.88	4.34	1.88
3	66	273.00	71.65	268.64	66	270.00	5.65	4.36	5.65	1.36
4	66	264.00	60.56	268.36	67	266.00	5.44	4.36	6.44	2.36
5	68	262.00	62.13	254.21	68	261.00	5.87	7.79	5.87	6.79
6	63	271.00	70.61	267.84	64	273.00	7.61	3.16	6.61	5.16
7	68	258.00	60.89	266.32	67	260.00	7.11	8.32	6.11	6.32
8	69	279.00	62.36	274.19	70	278.00	6.64	4.81	7.64	3.81
9	70	265.00	64.12	260.39	71	264.00	5.88	4.61	6.88	3.61
10	69	264.00	63.89	257.59	68	266.00	5.11	6.41	4.11	8.41
11	73	277.00	65.24	272.88	73	280.00	7.76	4.12	7.76	7.12
12	74	275.00	68.26	280.36	75	274.00	5.74	5.36	6.74	6.36
13	61	271.00	68.79	275.68	62	273.00	7.79	4.68	6.79	2.68
14	66	265.00	57.46	261.08	65	265.00	8.54	3.92	7.54	3.92
15	71	270.00	64.98	263.85	72	271.00	6.02	6.15	7.02	7.15
16	70	279.00	63.42	271.48	69	278.00	6.58	7.52	5.58	6.52
17	71	262.00	64.24	269.82	71	263.00	6.76	7.82	6.76	6.82
18	67	276.00	57.68	270.33	67	276.00	9.32	5.67	9.32	5.67
19	74	280.00	64.31	275.21	75	281.00	9.69	4.79	10.69	5.79
20	77	274.00	71.89	268.62	76	274.00	5.11	5.38	4.11	5.38
	Average Error						6.81	5.24	6.76	4.99

Table 8 compares the results of the 40-validated dip / dip direction measurements, with the mean error for the 40 dip / dip directions being ± 3.63° / ± 3.99° as shown in Table 8. Table 9 compares the results of the 20-validated dip / dip direction measurements, with the mean error for the 20 dip / dip directions being ± 6.81° / ± 5.24° as shown in Table 9. It has been analyzed that no data exceeds the tolerance range set in this study.
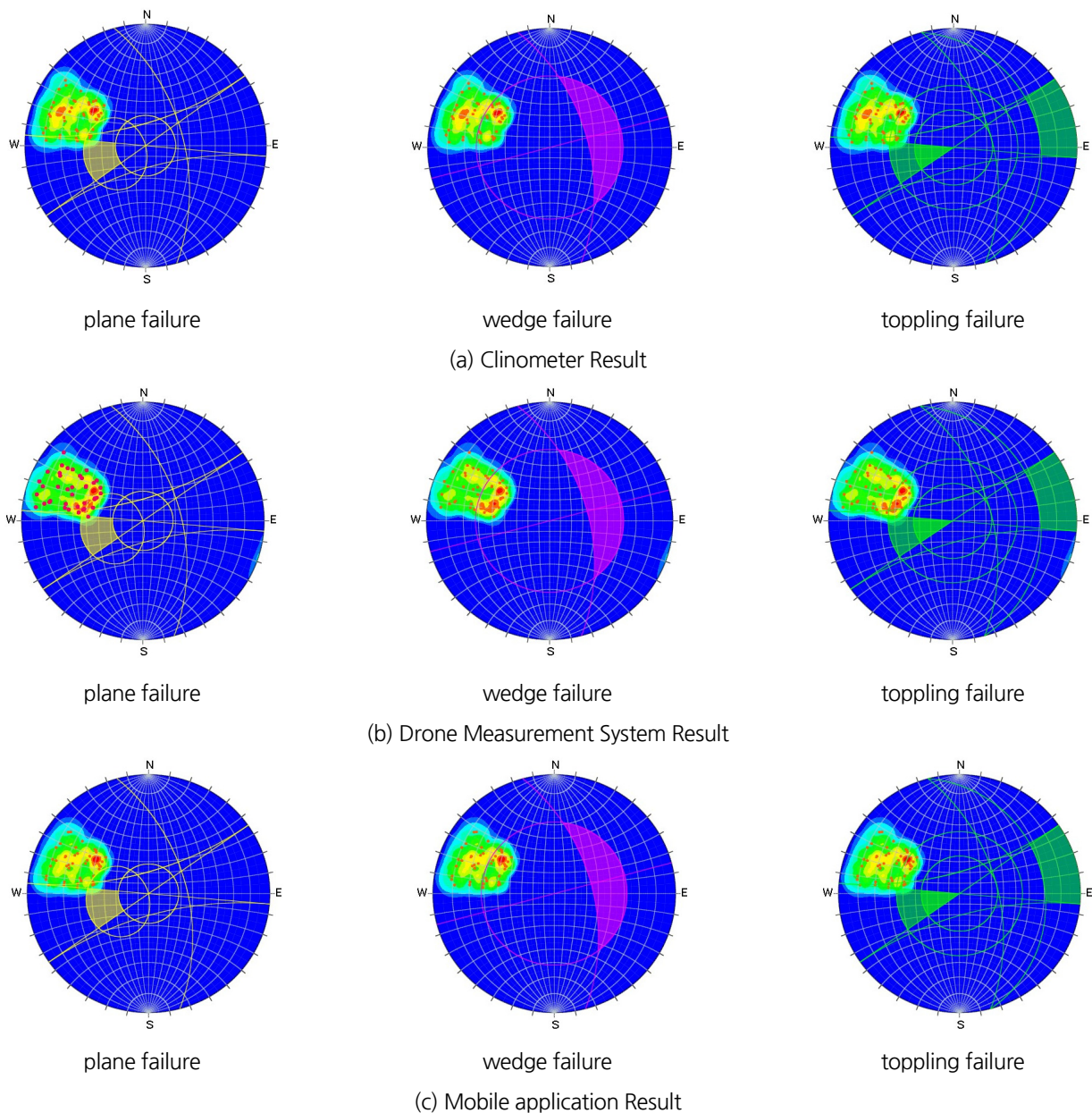
4.3 Analysis of Error Cause

In comparing the direction of the joint using the clinometer and the Drone Measure System the cause of the maximum error is determined by the difference in the measurement method of the joint surface.

It is assumed that, when using the Drone Measure System to obtain the joint orientation data, data errors are generated due to the effects of the refraction of the ultrasonic sensors, the effects of magnetic fields of the magnetic sensor, the drone's propeller noise, wind speed and the effects of temperature.
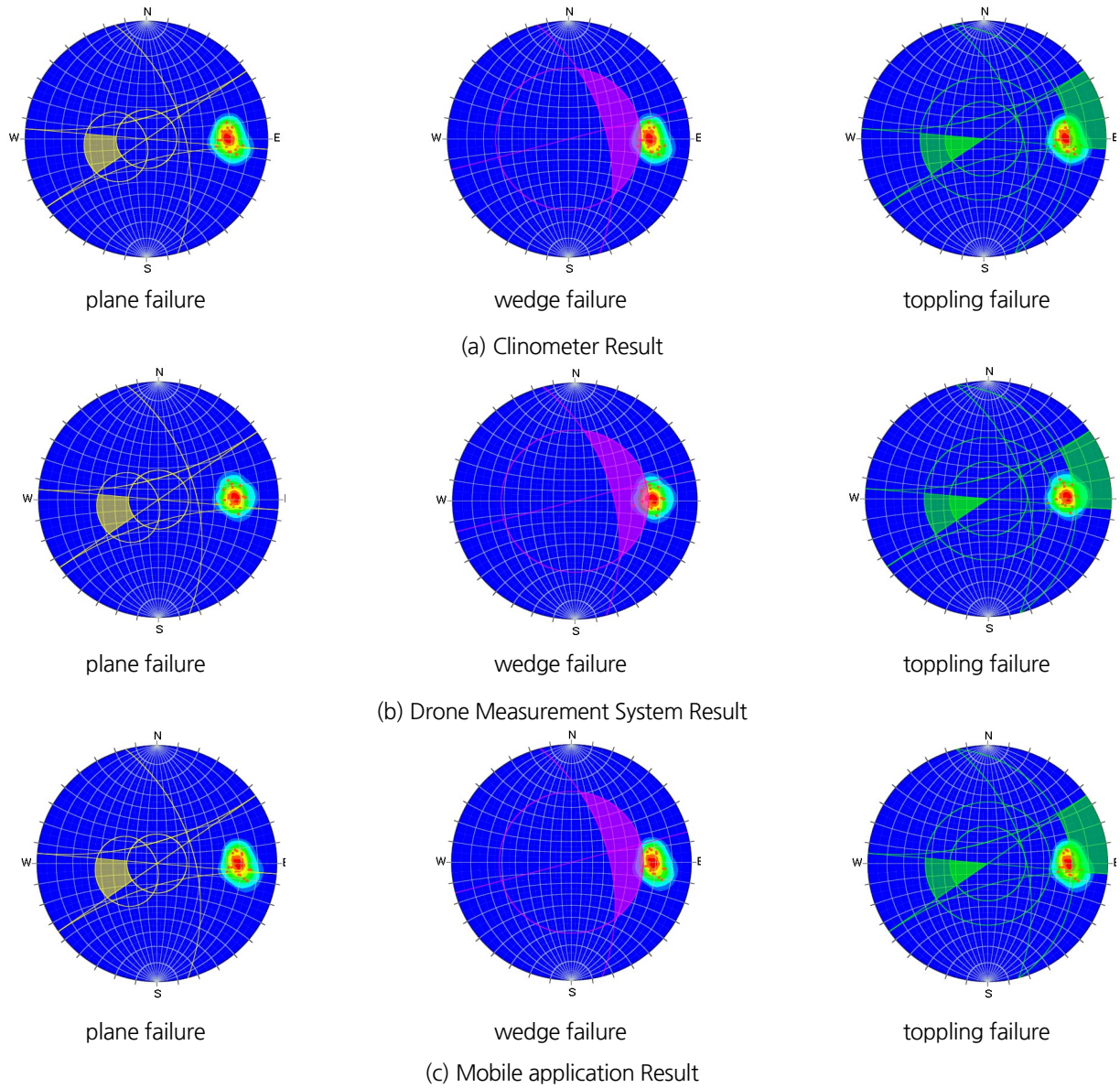
4.4 Analysis Result of the stereographic projection method

In the data analysis program, we measured the joint in the model slope and found that a total of 40 joints in the lab test and 20 joints in the field were measured, and depending on the orientation of the joint, a variety of joints were developed in the model slope.

Fig. 6 and Fig. 7 indicates the destructive type of each measuring instrument according to the measurement results of joint orientation in the lab test and in the field test. For each measuring instrument, the joint stability results are shown in Table 10 and Table 11.

plane failure wedge failure toppling failure

(a) Clinometer Result

plane failure wedge failure toppling failure

(b) Drone Measurement System Result

plane failure wedge failure toppling failure

(c) Mobile application Result

Fig. 6. Joint analysis using the stereographic projection method in the lab test

plane failure   wedge failure   toppling failure

(a) Clinometer Result

plane failure   wedge failure   toppling failure

(b) Drone Measurement System Result

plane failure   wedge failure   toppling failure

(c) Mobile application Result

Fig. 7. Joint analysis using the stereographic projection method in the field test

Table 10. Joint analysis result using the stereographic projection method in the lab test

Division	Clinometer	Drone measurement system	Mobile application
plane failure	stable	unstable	stable
wedge failure	unstable	unstable	unstable
toppling failure	stable	unstable	stable

Table 11. Joint analysis result using the stereographic projection method in the field test

Division	Clinometer	Drone measurement system	Mobile application
plane failure	stable	stable	stable
wedge failure	stable	stable	stable
toppling failure	unstable	unstable	unstable

5. Conclusions

In this study, the orientation of joint was measured automatically using the Drone Measure System, and the reliability of joint orientation using Drone Measure System was compared with the previous joint survey method. The results of the above study are as follows.

1. Since the test results are for the tolerance of joint orientation measured using a clinometer, the results of the comparison and analysis show that the deviation in the joint orientation measured by the Drone Measure system is ± 3° in the lab test ± 6° in the field test. The results are considered reliable data since they are within the tolerance range of ± 7° and ± 12° in the dip and dip direction set forth in this study.

2. When analyzing the causes of errors, it is analyzed that errors occurred due to differences in the measurement methods of joint. When measuring the joint orientation using the Drone Measure System, the effects of refraction on the joint surface, the effects of magnetic fields, and temperature are shown to cause errors in the lab test.

3. The joint measurement method using Drone Measure System secured the safety of the investigator and improved the efficiency of the survey by resolving the constraints of the previous joint survey method, namely, restriction of accessibility.

4. The results of the stereographic projection method show that the Drone Measure system shows conservative results compared to the previous methods in the lab test.

5. As a result of a field test, the problem of error in ultrasonic sensors caused by the drone's propeller noise should be suggested to use a low-noise propeller, consider the effects of wind speed during field measurement, and improve flight time and battery charge of the drone.

ACKNOWLEDGMENTS

REFERENCES

Ewan, V. J and West, G, 1981, Reproducibility of joint orientation measurements in rock, Transport and Road Research Laboratory supplementary report 702, 18P, International Journal of Rock Mechanics and Mining Science & Geomechanics Abstracts, Vol. 19, Issue 4, August 1982, Page 94.

Hagan, T. O., 1980, A case for Terrestrial photogrammetry in deep-mine rock structure studies, Int. J. Rock Mech. Min. Sci. 17, pp. 191-198.

Lee, S. H., 2016, Development of mobile software for field survey of geological structures, Seoul National University, pp. 29-34.

Moffitt, F. H. and E. M. Mikhail, 1980, 3rd Eds, Photogrammetry, Happer & Row Publisher, 648p.

Park, S. H., Lee, S. G., Lee, B. K. and Kim, C. H, 2015, A Study on Reliability of Joint Orientation Measurements in Rock Slop using 3D Laser Scanner, Tunnel and Underground Space, Vol. 25, No. 1, pp. 97-106.

Simon M., 2011, Programming Arduino Getting Started with Sketches, McGraw-Hill.

Son, Y. G., Kim, J. D., Jong, W. S., Kim, J. H. and Kim, K. S., 2014, Development of Joint Survey System using Photogrammetric, Tunnel and Underground Space, Vol. 24, No. 1, pp. 55-66.

XBee®/XBee-PRO® ZB RF Modules Datasheet (PDF). Digi International Inc. pp. 10, 2010.